Suppression of Mode Partition Noise in FP Laser by Frequency Modulation Non-Coherent Detection

Lei Xin, Jia Zhao, and Xun Li, *Senior Member, IEEE*

***Abstract*—We propose a frequency modulation (FM) non-coherent detection (NCD) scheme, attempting to suppress the mode partition noise (MPN) in fiber-optic communication systems with the Fabry-Perot (FP) semiconductor laser as the light source. The system comprises a FM transmitter with a directly modulated FP laser and a semiconductor optical amplifier, standard single mode fiber, and a NCD receiver with an optical slope filter as the FM to intensity modulation (IM) signal convertor placed in front of a conventional photodetector. In this configuration, the MPN is converted into a random frequency deviation by the transmitter and is reduced by the slope filter after fiber transmission. The FM signal is therefore less noisy after being converted back into the IM signal. With optimized parameter selections, our simulation result shows that the FM-NCD system allows a direct transmission span of 40 km for the 10 Gbps signal at 1577 nm, and 120 km for the 25 Gbps signal at 1310 nm, respectively, as opposed to a span of only 3 km and 10 km achievable by a conventional FP laser driven IM direct detection (DD) system for the corresponding signals at the corresponding wavelengths. Remarkably, our simulation result also shows that the performance of the FM-NCD system even surpasses that of a directly modulated distributed feedback laser driven IM-DD system, in which the maximum span is around 15 km and 60 km for 10 Gbps and 25 Gbps signals at 1577 nm and 1310 nm, respectively.**

***Index Terms*—FP lasers, frequency modulation, mode partition noise, non-coherent detection.**

I. Introduction

DRIVEN by internet-based applications and services, network traffic has grown explosively over decades, which leads to an ever-increasing demand on communication bandwidth [1]. In deployment of passive optical access networks and optical data communication links, cost reduction is the major pursuit [2]. Cost-effective optical components are therefore highly desirable in such systems and networks. The commonly exploited light source is the distributed feedback (DFB) laser, along which an optical isolator is often needed to prevent the output optical signal of the DFB laser from returning back, as otherwise its lasing status could be jeopardized. The cost of transmitters driven by the DFB laser are therefore relatively high. A low-cost alternative is the Fabry-Perot (FP) laser, along which the isolator is not necessary, as the total output power of the FP laser is less susceptible to the external optical feedback. However, its multiple (longitudinal) mode behavior, when combined with the fiber chromatic dispersion, creates the serious mode partition noise (MPN) problem that jeopardizes the system performance [3]. Hence the FP laser has to be excluded from being used in systems with data rates over 2.5 Gbps [4]. The MPN is caused by the longitudinal mode competition in the laser cavity where various modes compete for a common injected carrier population. The instantaneous power of each longitudinal mode in the laser diode exhibits large fluctuation, even though the total power of laser diode is nearly invariable [5], [6]. With such a set of fluctuating carriers, the pulse waveform at the receiver end varies randomly, as different carrier (longitudinal mode) travels at slightly different speed inside the fiber due to the chromatic dispersion. The distorted optical pulse waveform originated from the MPN reduces the signal-to-noise ratio (SNR) and degrades the bit-error-rate (BER); and is usually the dominating factor that limits the system performance [3], [7], and [8]. Suppressing the MPN by, e.g., replacing the FP laser with the single longitudinal mode DFB laser, therefore, becomes necessary in fiber-optic communication systems with data rates going beyond 2.5 Gbps. Single mode Fabre-Perot laser diodes (SMFP-LD) based on either coupled cavity [9], [10], slotted cavity [11]–[13], external cavity [14], or injection-locked [15] structures can also eliminate the MPN. External cavity and injection-locked SMFP-LDs are usually more expensive due to the hybrid packaging burden. Coupled or slotted cavity SMFP-LDs are more cost-effective due to their easier fabrication process as compared to DFB lasers, for there is no need to fabricate the grating and consequently no need to take one more growth step for grating coverage. Moreover, there is no facet grating phase involved, hence the yield of SMFP-LDs is usually higher. However, most SMFP-LDs suffer the mode instability problem, i.e., their lasing mode may hop with varying ambient temperature and/or bias current. As a result, their dynamic side mode suppression ratio (SMSR) is usually low, and they are vulnerable to temperature change. For these reasons, although SMFP-LDs have found applications in many other areas, they are not popular in fiber-optic access networks and optical datalinks.

Manuscript received August 15, 2021; revised September 28, 2021; accepted October 23, 2021. Date of publication October 29, 2021; date of current version November 22, 2021. This work was supported by the National Key Research and Development Programs of China under Grants 2018YFA0209000 and 2018YFB2200700. *(Corresponding author: Xun Li.)*

Lei Xin is with the School of Information Science and Engineering, Shandong University, Qingdao 266237, China (e-mail: lei_xin@mail.sdu.edu.cn).

Jia Zhao is with the Department of Electrical and Computer Engineering, McMaster University, Hamilton, ON L8S 4K1, Canada (e-mail: zhaojia@sdu.edu.cn).

Xun Li is with the Department of Electrical and Computer Engineering, McMaster University, Hamilton, ON L8S 4K1, Canada, and also with the School of Information Science and Engineering, Shandong University, Qingdao, Shandong 266237, China (e-mail: lixun@mcmaster.ca).

Digital Object Identifier 10.1109/JPHOT.2021.3123663

Other alternative methods have been proposed to reduce the MPN over the past years [16]–[18]. It was demonstrated that the MPN with its dominant components appearing in the low frequency band can be suppressed by the semiconductor optical amplifier acting as a high-pass filter [16]. Mode-locked lasers by incorporating a saturable absorber and a gain-modulated semiconductor optical amplifier (SOA) along with spectral filtering in an external cavity, were proposed respectively for effective reduction of the MPN [17]. Yet another approach exploited a built-in bandpass filter to narrow the spectral width of the FP laser hence to reduce the MPN [18]. All these approaches, however, either can hardly be justified in terms of their cost; or falls behind in system performance (due to incomplete elimination of the MPN), as compared to the DFB laser solution.

In this work, we propose a frequency modulation (FM) noncoherent detection (NCD) scheme in an attempt to suppress the MPN in systems with the FP laser as the light source. By exploiting the parasitic FM, also known as the chirp in a directly modulated FP laser, we may readily obtain the FM signal by eliminating the power fluctuation due to intensity modulation (IM) through a SOA with saturable amplification. After fiber transmission and upon the FM to IM conversion by a slope filter that suppresses the high frequency components, the signal is fed into a conventional photodetector (PD) for direct detection (DD). Since the MPN is translated into the random frequency deviation and will consequently be restrained by the slope filter, we expect that the MPN can be suppressed in such a system.

The rest of the paper is organized as follows. The FM-NCD system configuration is proposed in Section II. Our simulation model is described and validated in Section III. With optimized system parameters, numerical simulation results of two transmission examples, i.e., 10 Gbps signal at 1577 nm, and 25 Gbps signal at 1310 nm, are presented in Sections IV and V, respectively, in which the results of a directly modulated DFB laser driven conventional IM-DD systems are also shown for comparison. This work is finally summarized in Section VI.

II. System Configuration

A schematic diagram of the proposed FM-NCD system configuration for suppressing the MPN is shown in Fig. 1(a). In this system, a FP laser is directly modulated by the electric signal. Through the parasitic FM in accompanying with IM due to the chirp of the laser, we obtain an IM-FM optical signal. The power fluctuation of the IM-FM signal is then suppressed by the saturable amplification of an inline SOA. Thereby we obtain a relatively pure FM optical signal. After fiber transmission, we transform the FM signal back into the IM signal by exploiting an optical slope filter, rather than by taking the conventional coherent detection approach [19] for cost-effectiveness. The IM signal is finally converted back into the electric signal by a conventional photodetector. It is crucial to limit the bandwidth of the optical slope filter to below half of the mode spacing and have it aligned with the center longitudinal mode frequency of the FP laser. As such, all side mode frequencies of the FP laser will be cut off with the FM signal carried by only the center mode being converted back into the IM signal. We expect that

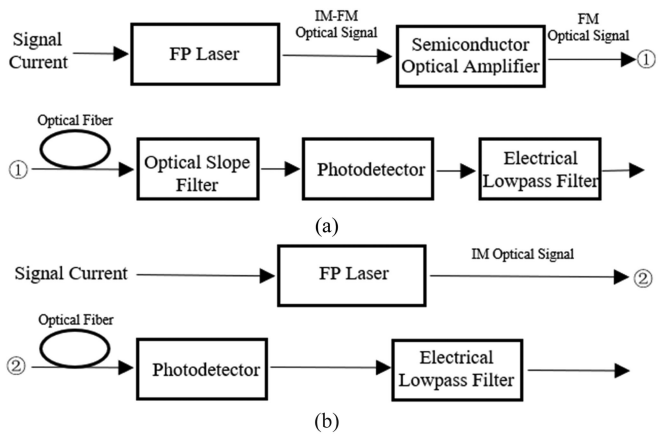

Fig. 1. Schematic diagram of system configurations: (a) the proposed FM-NCD system and (b) the conventional IM-DD system for comparison.

the removal of the fluctuated side modes (exhibited as varying frequencies in sidebands of the FM signal) will restrain their contribution to waveform distortion. Moreover, the FM signal is designed to pass through the falling tail, rather than the leading tail, of the optical slope filter. Hence symbol 0 and 1 are inverted. Such an arrangement is advantageous since the center mode fluctuation (exhibited as the random deviation of the FM signal center frequency) at symbol 1 will be suppressed by the heavy loss at the edge of the filter with a deep slope. For comparison purpose, we have also shown a conventional IM-DD system configuration in Fig. 1(b).

III. Simulation Modal

A. Optical Transmitter

In modeling of the proposed system, the FP laser is described by multimode rate equations [3], [20], and [21]:

$$\frac{dN\left(t\right)}{dt}=\frac{I\left(t\right)}{eV}-\frac{N\left(t\right)}{\tau_c}-\sum_i\frac{\Gamma v_g g_i\left(N\right)S_i\left(t\right)}{1+\varepsilon S_{tot}}+F_N\left(t\right), \tag{1}$$

$$\frac{dS_i\left(t\right)}{dt}=\left[\frac{\Gamma v_g g_i\left(N\right)S_i\left(t\right)}{1+\varepsilon S_{tot}}-\frac{1}{\tau_p}\right]S_i\left(t\right)+R_{sp,i}\left(t\right)+F_s\left(t\right), \tag{2}$$

$$\frac{d\Phi_i\left(t\right)}{dt}=0.5\alpha_{LEF}\left[\Gamma v_g g_i\left(N\right)-\frac{1}{\tau_p}\right]+F_\Phi\left(t\right), \tag{3}$$

where the material optical gain is expressed as

$$g_i\ \left(N\right)=\ a\ln\left(N/N_0\right)\left[1-0.5(i\Delta\lambda_D/\Delta\lambda_G)^2\right]. \tag{4}$$

In above equations, the subscript i is assigned to corresponding variables in the i^{th} lasing (longitudinal) mode, where $i=0,\mp1,\mp2,\ldots,\mp M$, with a total number of longitudinal modes assumed as $2M+1$. Other variables, parameters, and physical constants are defined as: $N(t)$ the carrier density, $I(t)$ the injected current, e the electron charge, V the active region volume, τ_c the carrier lifetime, Γ the optical confinement factor, $v_g=c/n_g$ the group velocity, c the speed

of light, n_g the group index, ε the nonlinear gain suppression coefficient, $S_i(t)$ the photon density of the i^{th} longitudinal mode, $S_{tot} = \sum_i S_i$ the total photon density in all modes, $\tau_p = 1/\{v_g[\alpha + 1/(2L)\ln(1/R_f R_b)]\}$ the photon lifetime, α the optical modal loss, L the laser cavity length, R_f and R_b the reflectivity of the front and back facet, respectively, $R_{sp,i} = Kn_{sp}\Gamma v_g g_i(N)/(1+\varepsilon S_{tot})\ /V$ the spontaneously emitted photon density rate, K Petermann's factor, n_{sp} the population inversion factor, a the material gain coefficient, N_0 the transparent carrier density, $\Delta\lambda_D = \lambda_0^2\ /(2n_g L)$ the longitudinal mode spacing, λ_0 the peak gain (center lasing) wavelength, $\Delta\lambda_G$ the gain profile width, $\Phi_i(t)$ the phase of the i^{th} longitudinal mode optical field, and α_{LEF} the linewidth enhancement factor. Following the definition in [3] and [20], the Langevin noise terms $F_N(t)$, $F_S(t)$, and $F_\Phi(t)$ are stochastic processes with their characteristics given by:

$$\langle F_N(t)\rangle = \langle F_S(t)\rangle = \langle F_\Phi(t)\rangle = 0, \tag{5}$$

$$\langle F_u(t)\, F_v(t')\rangle = 2D_{uv}\delta(t-t'), \tag{6}$$

where the angle brackets denote the ensemble average and $\delta(t-t')$ Dirac's delta function. D_{uv} are the diffusion coefficients associated with the corresponding noise sources, with subscript u and v indicating N, S, and Φ. They can be explicitly expressed as [20]:

$$D_{NN} = N/(\tau_c V) + \sum_i R_{sp,i} S_i, \tag{7a}$$

$$D_{S_i S_i} = R_{sp,i}\, S_i, \tag{7b}$$

$$D_{NS_i} = D_{S_i N} = -R_{sp,i} S_i, \tag{7c}$$

$$D_{\Phi_i\Phi_i} = R_{sp,i}\,/(4S_i), \tag{7d}$$

$$D_{N\Phi_i} = D_{\Phi_i N} = D_{S\Phi_i} = D_{\Phi_i S} = 0. \tag{7e}$$

In solving above rate equations in the time domain, we have implemented the Langevin noise terms in time interval Δt as [22]:

$$F_N(t) = \sqrt{2D_{NN}/\Delta t}\, x_N, \tag{8a}$$

$$F_{S_i}(t) = \frac{D_{NS_i}}{D_{NN}} F_N(t) + \sqrt{2\frac{D_{S_iS_i} - {D_{NS_i}}^2/D_{NN}}{\Delta t}}\, x_{S_i}, \tag{8b}$$

$$F_{\Phi_i}(t) = \sqrt{2D_{\Phi_i\Phi_i}/\Delta t}\, x_{\Phi_i}, \tag{8c}$$

where x_N, x_{S_i}, and x_{Φ_i} are normalized independent Gaussian random variables with zero mean and unit standard deviation.

Rate (1)-(3) are solved by the 4th-order Runge-Kutta algorithm [23]. The optical power carried by each longitudinal mode can be linked to the photon density of the corresponding mode through [22], [24]:

$$P_i(t) = \frac{hv_i}{2}\ \frac{(1-R_f)\ln[1/(R_f R_b)]}{1-R_f+(1-R_b)\sqrt{R_f/R_b}}\frac{c}{n_g L} S_i(t)\, V, \tag{9}$$

with h indicating Planck's constant and v_i the optical frequency of the i^{th} longitudinal mode.

With parameters of a typical 1577 nm FP laser summarized in Table I, its performance under 10 Gbps direct modulation is calculated. The dots in Fig. 2 show the calculated probability density functions (PDF) of a few selected longitudinal modes by following the method described in [22] and [25]. The solid lines in Fig. 2 are PDF curves obtained by a theoretical model

TABLE I
PARAMETERS OF THE FP LASER

Name	Symbol	Value	Unit
Active region width	w	2	μm
Total quantum well thickness	d	0.04	μm
Laser cavity length	L	150	μm
Optical confinement factor	Γ	0.06	
Carrier lifetime	τ_c	0.1	ns
Group index	n_g	3.6	
Material gain coefficient	a	3000	cm^{-1}
Transparent carrier density	N_0	6×10^{17}	cm^{-3}
Gain profile width	$\Delta\lambda_G$	100	nm
Peak gain wavelength	λ_0	1577	nm
Nonlinear gain compression coefficient	ε	2.5×10^{-17}	cm^3
Optical modal loss	α	10	cm^{-1}
Reflectivity of front facet	R_f	0.3	
Reflectivity of back facet	R_b	0.9	
Petermann's factor	K	1	
Population inversion factor	n_{sp}	1.7	
Linewidth enhancement factor	α_{LEF}	8	
Total number of longitudinal modes	$2M+1$	19	

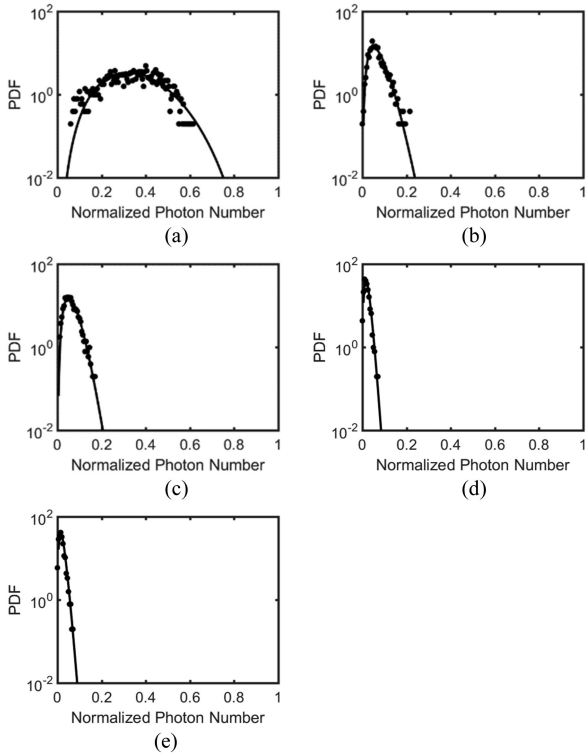

Fig. 2. Probability density functions (PDF) of (a) the central mode S_0 and a few side modes: (b) S_{-2}, (c) S_2, (d) S_{-4}, and (e) S_4. The dots are the calculated PDFs by the multimode rate equation model. The solid lines are PDF curves obtained by a theoretical model [26].

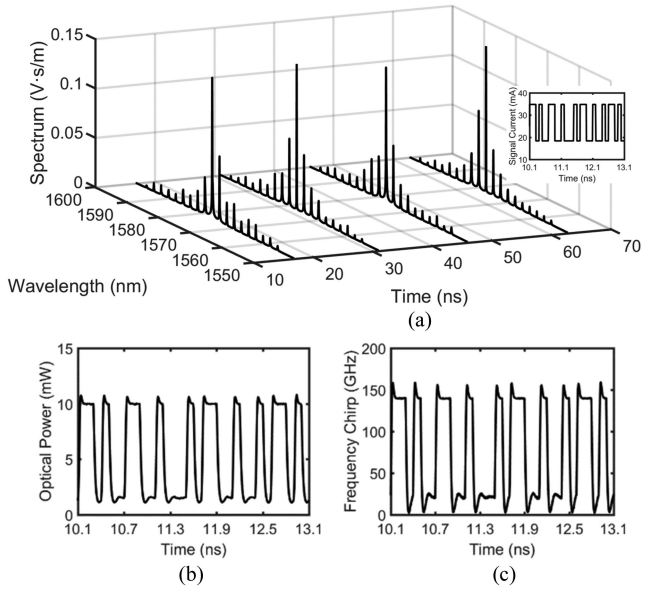

Fig. 3. Characteristics of the FP laser: (a) the time-resolved spectrum of the FP laser under direct modulation with the applied signal current shown in the inset, where the spectral time window is set to 100 ps, (b) the total output optical power of the FP laser, and (c) the frequency chirp of the central mode S_0.

[26]:

$$p\ (a_i) = \frac{a_i^{(\xi\overline{a_i}-1)}(1-a_i)^{[\xi(1-\overline{a_i})-1]}}{B\left[\xi\overline{a_i}, \xi\left(1-\overline{a_i}\right)\right]}\ , \tag{10}$$

where $a_i = S_i/S_{tot}$ is the relative photon density in the i^{th} longitudinal mode, $B(x, y)$ the Beta-function, $\overline{a_i} = \sum_i a_i/(2M+1)$ the average value of a_i , and $\xi = 1/k^2 - 1$ the mode partition coefficient with the corresponding k-factor defined as:

$$k^2 = \left(\overline{a_i^2} - \overline{a_i}^2\right) / \left(\overline{a_i} - \overline{a_i}^2\right). \tag{11}$$

The simulated MPN characteristics are in good agreement with the theory as evidenced by Fig. 2, which validates our multimode rate equation model for the FP laser. Other device characteristics obtained from this model are shown in Fig. 3. Despite the severe power fluctuation of each individual mode under direct modulation as shown in Fig. 3(a), the total optical power in each symbol-1 pulse remains almost unchanged, as exhibited in Fig. 3(b). For a fair comparison with the conventional IM-DD system, the operating condition is such chosen that the output optical power and extinction ratio (ER) of the optical transmitter satisfy the ITU standard for 10-Gigabit-capable passive optical networks (XG-PON) [27], although it is the parasitic frequency modulation (chirp), rather than the intensity modulation itself, will be used for signal transmission. Fig. 3(c) clearly shows the parasitic frequency modulation due to the carrier induced frequency chirping as modeled by the phase rate (3).

Since a pure FM signal is required by the FM-NCD system, we need to pass the IM-FM signal from the directly modulated FP laser further through a SOA for saturable amplification. A physics-based model [28]–[30], as briefed in Appendix A, has been used to simulate the SOA operated under its saturation mode. The SOA equations are solved numerically [31] with its parameters summarized in Table II. Fig. 4(a) shows that the total output optical power can indeed be saturated by the SOA with minor fluctuations. As such, the output of the SOA becomes a rather pure FM signal, as evidenced by Fig. 4(b). The spectrum of the central mode has two main peaks, corresponding to symbol-0 (the one on the left) and symbol-1 (the one on the right) lasing frequencies, respectively, which carries the signal information.

TABLE II
PARAMETERS OF THE SOA

Name	Symbol	Value	Unit
Active region width	w	2	μm
Total quantum well thickness	d	0.04	μm
Active region length	L	0.1	cm
Optical confinement factor	Γ	0.08*	
Carrier lifetime	τ_c	0.5*	ns
Group index	n_g	3.6	
Material gain coefficient	a	3000	cm^{-1}
Transparent carrier density	N_0	6×10^{17}	cm^{-3}
Gain profile width	$\Delta\lambda_G$	100	nm
Peak gain wavelength	λ_0	1577	nm
Nonlinear gain compression coefficient	ε	2.5×10^{-17}	cm^3
Optical modal loss	α	10	cm^{-1}
Reflectivity of front facet	R_f	0.001	
Reflectivity of back facet	R_b	0.001	
Effective index without injection	n_{eff}^0	3.18	
Spontaneous coupling factor	γ	0.01	
Linewidth enhancement factor	α_{LEF}	3	
Injected current	I	100	mA

*: requirements of reduced saturation power.

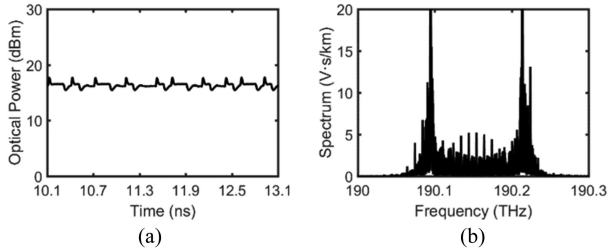

Fig. 4. Characteristics of the FM transmitter: (a) the total output optical power and (b) the spectrum of the central mode S_0 after saturable amplification of the SOA.

B. Fiber-Optic Channel

As briefed in Appendix B, the transmission of the optical signal is described by the nonlinear Schrodinger equation [32], which can readily be solved by, e.g., the split-step method [33], [34]. In our simulation example, the G.652.D single mode fiber (SMF) with a loss of 0.2 dB/km and a dispersion $(D = -2\pi c\beta_2/\lambda^2)$ of 18 ps/(nm.km) at 1577 nm is used. Since the proposed system is not for long haul transmission, the fiber nonlinearity, the third and higher order dispersions are all neglected. Under this condition, a single step in the numerical solver returns the fiber transmission result.

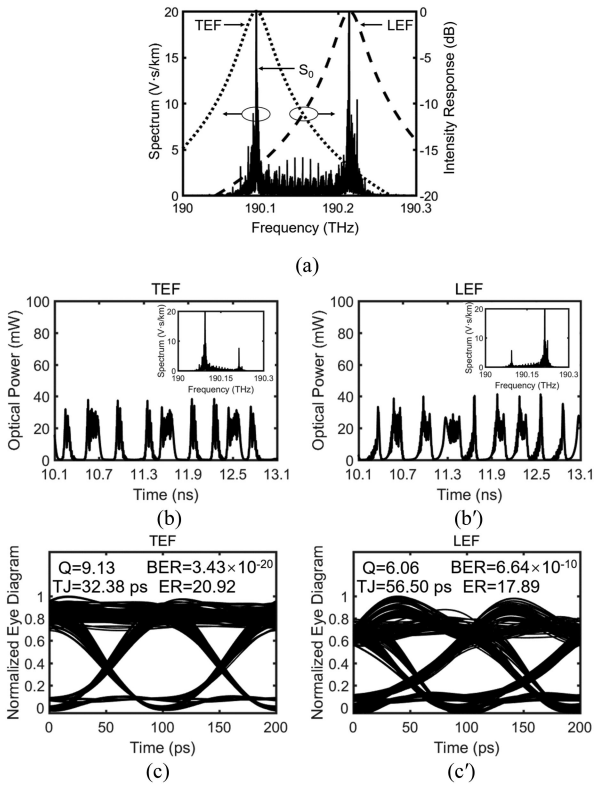

Fig. 5. System performance comparison between the TEF and LEF approach: (a) the spectra of the central mode S_0 after 10-km optical fiber transmission, and frequency responses of the TEF and LEF, (b) and (b′) the waveforms and spectra (shown in the insets) of the optical signal after slope filtering by the TEF and LEF, respectively, and (c) and (c′) the eye-diagrams of the optical signal after slope filtering by the TEF and LEF, respectively, with the extracted effective SNR (Q), bit-error-rate (BER), total time jitter (TJ), and extinction ratio (ER) shown at the top of each figure.

C. Optical Receiver

As the component that converts the FM signal back to the IM signal, the optical slope filter plays a crucial role in the FM-NCD system. Without losing much generality, we consider a 2nd order optical bandpass filter in the form of:

$$H_{sl}\ (j\omega) = \ Aj\omega\omega_d / \left[(j\omega)^2 + j\omega\omega_d + \omega_0^2\right], \qquad (12)$$

which can be practically realized by, e.g., multiple dielectric layer coatings. Depending on choosing the rising or falling tail of its frequency response, we can obtain the required optical slope filtering function either through the leading-edge filter (LEF) or the tailing-edge filter (TEF). As shown in Fig. 5(a), with a common $A = 1$, $\omega_d = 217.66 \times 10^9$ rad/s, the LEF tuned at $\omega_0 = 1.1952 \times 10^{15}$ rad/s and TEF tuned at $\omega_0 = 1.1944 \times 10^{15}$ rad/s suppresses the low and high frequency band of the FM optical signal, respectively. Fig. 5(b) and (b′) give the optical waveforms, and Fig. 5(c) and (c′) the eye-diagrams, of the optical signal after being filtered by the TEF and LEF, respectively. The quality of the eye-diagram can be quantitatively evaluated by those extracted parameters inserted at the top of each corresponding figure. The effective SNR is calculated by:

$$Q \ = \ (I_1 - I_0) \,/\, (\sigma_1 + \sigma_0)\,, \qquad (13)$$

where I_1 and I_0, and σ_1 and σ_0, denoted as the averages and variances of symbol-1 and symbol-0 signal at the decision instant, respectively, are directly obtained from the eye-diagram. Consequently, the BER is found as:

$$BER \ = \ 1/2erfc\left(Q/\sqrt{2}\right), \qquad (14)$$

with $erfc()$ denoting the complementary error function. The total time jitter (TJ) is calculated by the model in [35], at a BER of 10^{-3} as required by the receiver of the optical network unit (ONU) in XG-PON according to the standard in [27]. The ER is calculated by I_1/I_0. Our simulation shows that the TEF is superior to the LEF. The MPN induced power fluctuation is positively correlated with the power, i.e., power fluctuation is severer in symbol-1 than in symbol-0, which consequently causes a larger frequency deviation in symbol-1 than in symbol-0. Since the TEF retains low-frequency components and suppresses high-frequency components, it introduces less fluctuation in converting the FM signal into the IM signal. On the contrary, the LEF retains the high-frequency components and suppresses the low-frequency components, which leads to greater fluctuation to the converted IM signal. To eliminate extra frequency deviations, we need to cut off all the side modes. This can practically be achieved by cascading yet another optical bandpass filter with its bandwidth chosen less than the FP mode spacing. In our simulation model, we have simply assumed that the bandwidth of the TEF is less than half of the mode spacing. Thereby all side mode frequencies are eliminated. We have also studied the impact of the rolling rate of the slope in the TEF on system performance. With $A = 1$ and $\omega_0 = 1.1944 \times 10^{15}$ rad/s, the TEF's ω_d is chosen as 362.76×10^9 rad/s, 290.21×10^9 rad/s, 217.66×10^9 rad/s, and 145.10×10^9 rad/s, respectively. They are denoted by symbols "S", "M", "F", and "UF", meaning that the rolling rate of the TEF's slope is "slow", "medium", "fast", and "ultra-fast", respectively. Shown in Fig. 6, the eye-diagrams of the FM signal after 30-km optical fiber transmission indicate that the rolling rate of the TEF's slope has an optimum value. We find that the TEF with a fast-rolling slope marked as "F" gives the best system performance. This is understandable as a slow-rolling slope will not sufficiently mitigate the effect of the MPN on symbol-1. An ultra-fast rolling slope, however, jeopardizes the signal fidelity as the signal is severely distorted by the ultra-narrow bandwidth associated with the ultra-fast rolling slope.

After being converted from the FM signal by the TEF, the optical IM signal is directly detected by a normal photodetector. The photocurrent is calculated by $I_{PD} = RP_{in}$ with *R* and P_{in} indicating the responsivity of the photodetector (0.9 A/W in our simulation) and the input optical power to the photodetector, respectively. A common 6th order Butterworth electrical lowpass filter with the cutoff frequency at 8 GHz is adopted after photodetection for noise suppression outside of the signal baseband.

IV. Transmission of the 1577 nm 10 Gbps Signal

With the proposed FM-NCD system configured in Fig. 1 and with the parameters for optical fiber and other functional blacks chosen in Section III, we have simulated the performance of

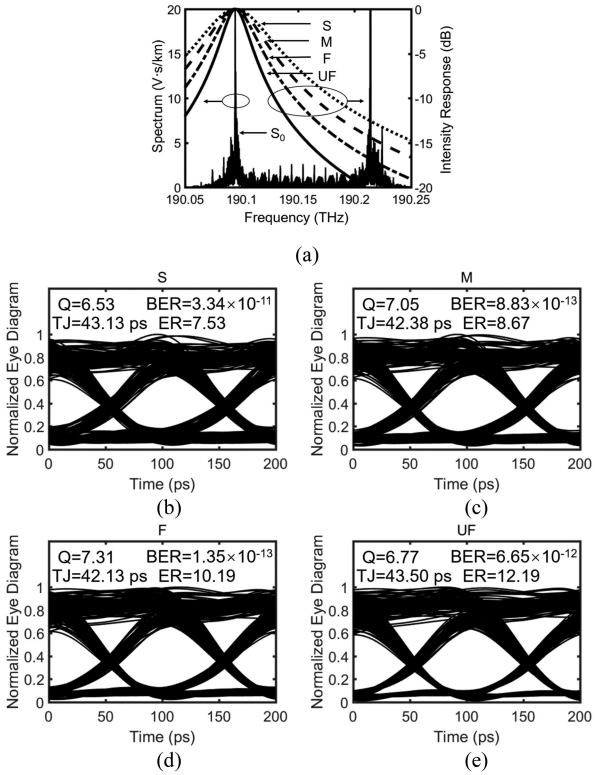

Fig. 6. System performance of the TEF with different slope rolling rate: (a) the spectrum of the central mode S_0 after 30-km optical fiber transmission, and frequency responses of the TEF denoted by "S", "M", "F", and "UF", (b)–(e) eye diagrams of the optical signal after slope filtering by the "S", "M", "F", and "UF" TEF, respectively, with the extracted effective SNR (Q), bit-error-rate (BER), total time jitter (TJ), and extinction ratio (ER) shown at the top of each figure.

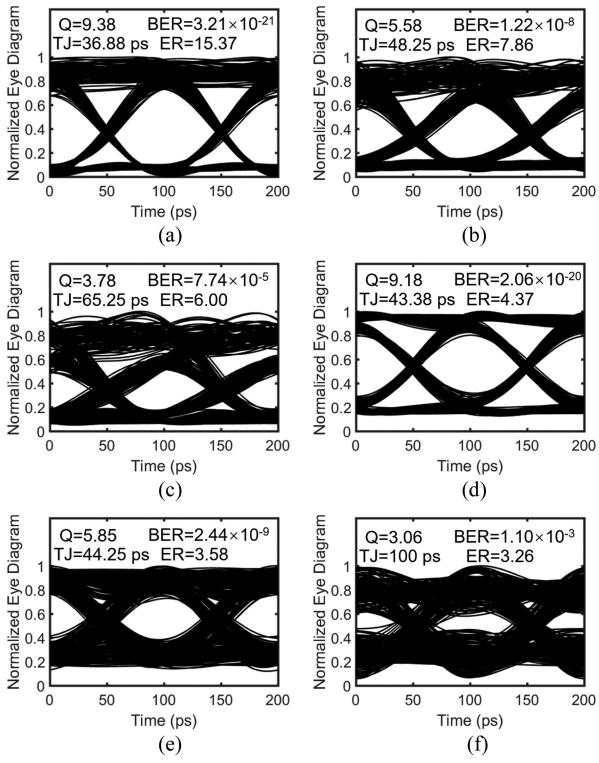

Fig. 7. Eye diagrams of the 1577 nm 10 Gbps optical signal after (a) 20-km, (b) 40-km, and (c) 60-km transmission in the proposed FM-NCD system, respectively; as a comparison, the eye diagrams of the same signal in a FP laser driven IM-DD system are also shown after only 1-km (d), 3-km (e), and 5-km (f) transmission, with the FP laser modulation current and its output optical signal waveforms given in the inset of Fig. 3(a) and Fig. 3(b), respectively. The extracted effective SNR (Q), bit-error-rate (BER), total time jitter (TJ), and extinction ratio (ER) are also shown at the top of each eye-diagram.

a 1577 nm 10 Gbps transmission system. The obtained eye diagrams are shown in Fig. 7. It is found that the proposed FM-NCD system allows the 1577 nm 10 Gbps signal to transmit over 40 km, as opposed to only about 3 km achievable by a conventional IM-DD system driven by a FP laser. To demonstrate the superiority of the proposed FM-NCD system, a DFB laser driven conventional IM-DD system is further simulated with the model described in Appendix C and parameters presented in Table III. As shown in Fig. 8 by the eye diagrams, the maximum span of the DFB laser driven IM-DD system is about 15 km for the same 1577nm 10 Gbps signal, which indicates that the performance of the proposed FM-NCD system driven by a FP laser (plus an extra SOA and a passive optical slope filter) even surpasses that of the IM-DD system driven by a DFB laser.

TABLE III
PARAMETERS OF THE DFB LASER

Name	Symbol	Value	Unit
Bragg grating period	Λ	248	nm
Active region width	w	2	μm
Total quantum well thickness	d	0.04	μm
Active region length	L	150	μm
Optical confinement factor	Γ	0.06	
Grating coupling coefficient	κ	100	cm^{-1}
Carrier lifetime	τ_c	0.1	ns
Group index	n_g	3.6	
Material gain coefficient	a	3000	cm^{-1}
Transparent carrier density	N_0	6×10^{17}	cm^{-3}
Peak gain wavelength	λ_0	1577	nm
Nonlinear gain suppression coefficient	ε	2.5×10^{-17}	cm^3
Optical modal loss	α	10	cm^{-1}
Reflectivity of front facet	R_f	0.3	
Reflectivity of back facet	R_b	0.95	
Effective index without injection	n_{eff}^0	3.18	
Spontaneous coupling factor	γ	1×10^{-4}	
Linewidth enhancement factor	α_{LEF}	3	
IIR filter coefficient	η	0.002	

V. TRANSMISSION OF THE 1310 NM 25 GBPS SIGNAL

By exploiting the same configuration and model described in Sections II and III, we have also simulated the performance of the proposed FM-NCD system for transmission of the 1310 nm 25 Gbps signal, with all parameters summarized in Table IV. Following the standard in [36], the TJ shown at the top of each eye-diagram in Fig. 9 is calculated at a BER of 5×10^{-5}, as required by the receiver in optical datalinks. Comparison among the eye-diagrams in Fig. 9 again reveals that the proposed FM-NCD system not only offers a better performance than the FP laser driven conventional IM-DD system, but is also superior than the DFB laser driven IM-DD system, as evidenced by the maximum allowed transmission span of 120 km for the FM-NCD system, 10 km for the FP laser driven IM-DD system, and 60 km for the DFB laser driven IM-DD system, respectively.

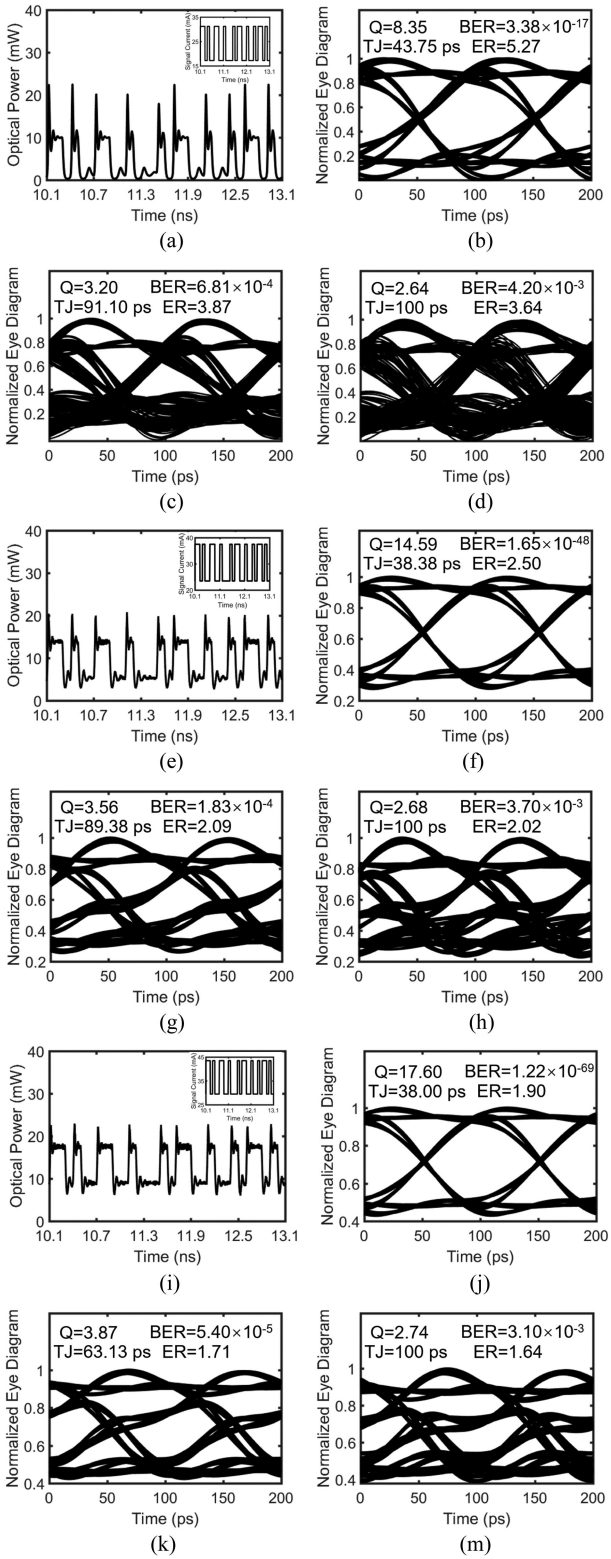

Fig. 8. Eye diagrams of the 1577 nm 10 Gbps optical signal after 5-km (b), (f), and (j), 15-km (c), (g), and (k), and 20-km (d), (h), and (m) transmission in a DFB laser driven IM-DD system, respectively, with the extracted effective SNR (Q), bit-error-rate (BER), total time jitter (TJ), and extinction ratio (ER) shown at the top of each figure, (a), (e) and (i) the optical signal waveform launched by the directly modulated DFB laser with the applied signal current shown in the inset.

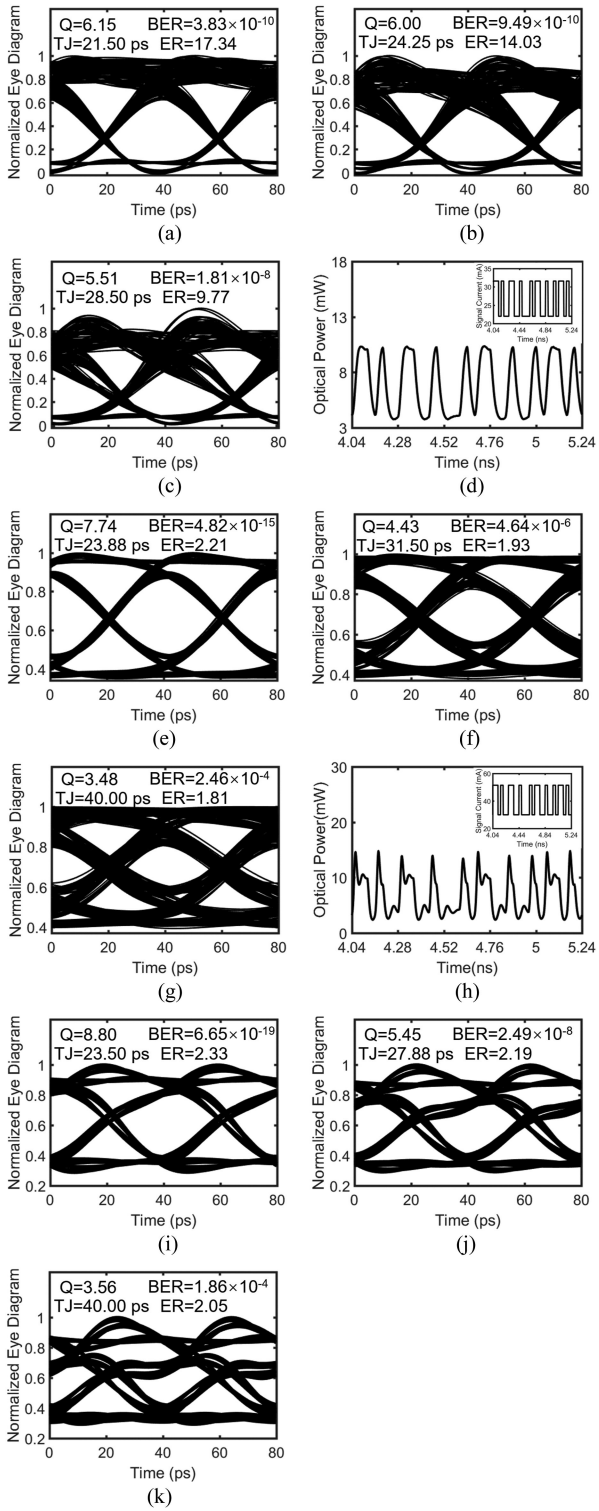

Fig. 9. Eye diagrams of the 1310 nm 25 Gbps optical signal after 70-km (a), 120-km (b), and 170-km (c) transmission in the proposed FM-NCD system, respectively; as comparisons, the eye diagrams of the same signal in a FP laser driven IM-DD system are shown after only 5-km (e), 10-km (f), and 15-km (g) transmission, and the eye diagram of the same signal in a DFB laser driven IM-DD system are also shown after 50-km (i), 60-km (j), and 70-km (k) transmission, respectively; (d) and (h) the optical signal waveforms launched by the directly modulated FP and DFB lasers, with the applied signal currents shown in the insets, respectively. The extracted effective SNR (Q), bit-error-rate (BER), total time jitter (TJ), and extinction ratio (ER) are also shown at the top of each eye-diagram.

TABLE IV
FM-NCD SYSTEM PARAMETERS FOR 1310 nm 25 Gbps OPTICAL SIGNAL TRANSMISSION

Device	Name	Symbol	Value	Unit
FP laser	Peak gain wavelength	λ_0	1310	nm
DFB laser	Bragg grating period	Λ	203	nm
	Peak gain wavelength	λ_0	1310	nm
	Effective index without injection	n_{eff}^0	3.21	
SOA	Peak gain wavelength	λ_0	1310	nm
	Effective index without injection	n_{eff}^0	3.21	
Optical fiber	Fiber loss	α	0.35	dB/km
	Dispersion parameter	D	1	ps/(nm. km)
LEF		A/K	1.6324 $\times 10^{11}$	
		B	2.0682 $\times 10^{30}$	
Electrical lowpass filter	Cutoff frequency		20	GHz

Other parameters are identical to those used in Tables I-III.

Under the same IM scheme (i.e., both directly modulated without any signal conversion), the system performance of the DFB laser will surely surpass that of the FP laser. The fact that the FM-NCD system with a FP laser shows a better performance than the conventional IM-DD system with a DFB laser indicates that the FM scheme is superior, if the MPN in FP and the chirp in DFB are the limiting factors in transmission due to the fiber chromatic dispersion.

VI. CONCLUSION

A FM-NCD fiber-optic communication system is proposed by exploiting the parasitic frequency modulation (chirp) of a directly modulated FP laser and a SOA for saturable amplification. After fiber transmission, the FM signal is converted back into a normal IM signal by a passive optical slope filter. Such a system can effectively suppress the MPN as evidenced by our numerical simulation results. More specifically, the proposed FM-NCD system allows a maximum transmission span of 40 km for the 1577 nm 10 Gbps signal, and 120 km for the 1310 nm 25 Gbps signal, as opposed to 3 km and 10 km achievable by a FP laser driven, or 15 km and 60 km achievable by a DFB laser driven conventional IM-DD system, respectively. Hence the FM-NCD system will become the power- rather than the bandwidth- limited system.

In the passive optical network (PON) based telecommunication access networks, external modulated lasers (EMLs) are usually used as the downstream source in the optical line terminal (OLT), as the DFB lasers cannot send 10 Gbps signal for over 20 km at 1577 nm as required by the PON system standard, due to the DFB chirp (parasitic frequency modulation) and the fiber chromatic dispersion [37]. EML needs butt-joint regrowth or selective area growth to monolithically integrate the DFB with the electro-absorption modulator (EAM), which is a complicated technique and still suffers low yield on current fabrication technology [38]. In the proposed FM-NCD system, on the transmitter side, the FP-LD and SOA are both mature devices and can readily be monolithically integrated without regrowth, since the active region of the FP-LD and SOA can be identical, with their electrodes for current injection being separated only. On the receiver side, only an extra optical slope filter is needed. However, it is a purely passive device and can be made by directly coating on the photodetector surface. The overall expense of the FP-SOA plus the optical slope filter can be made lower than that of the EML. In short to medium range 25 Gbps optical datalinks at 1310 nm with a span of several to more than ten kilometers, directly modulated DFBs are commonly used for its cost-effectiveness as compared to EML. Since there is no grating required, a combination of the FP-SOA plus optical slope filter can be made even more cost-effective than the combination of the DFB plus isolator. Besides, we can expect a higher yield of the FP-SOA as compared to the DFB for there is no grating facet phase uncertainty involved. Since there is neither expensive component nor complicated technology involved, the FM-NCD system can be appealing as a cost-effective approach for optical signal transmission in optical fiber based passive optical access networks and in optical datalinks.

APPENDIX A

The numerical model that we have adopted to describe the SOA is given as [28]–[30]:

$$\frac{dN(z,t)}{dt} = \frac{I}{eV} - \frac{N(z,t)}{\tau_c} - v_g \sum_{i=-M}^{M} \frac{P_s(z,t,\lambda_i)\, g(z,t,\lambda_i)}{1+\varepsilon P_{tot}(z,t)}, \tag{15}$$

$$\left(\frac{1}{v_g}\frac{\partial}{\partial t} + \frac{\partial}{\partial z}\right) F(z,t,\lambda_i) = \left\{ j\left[\frac{1}{2}\alpha_{LEF}\Gamma g(z,t,\lambda_i)\right] + \frac{1}{2}\left[\frac{\Gamma g(z,t,\lambda_i)}{1+\varepsilon P_{tot}(z,t)} - \alpha\right]\right\} \cdot F(z,t,\lambda_i) + \tilde{s}^f(z,t,\lambda_i), \tag{16}$$

$$\left(\frac{1}{v_g}\frac{\partial}{\partial t} - \frac{\partial}{\partial z}\right) R(z,t,\lambda_i) = \left\{ j\left[\frac{1}{2}\alpha_{LEF}\Gamma g(z,t,\lambda_i)\right] + \frac{1}{2}\left[\frac{\Gamma g(z,t,\lambda_i)}{1+\varepsilon P_{tot}(z,t)} - \alpha\right]\right\} \cdot \mathrm{R}(z,t,\lambda_i) + \tilde{s}^r(z,t,\lambda_i), \tag{17}$$

where $N(z,t)$ is the carrier density, I the injected current, e the electron charge, V the active region volume, τ_c the carrier lifetime, $v_g = c/n_g$ the group velocity, c the speed of light, n_g the group index, $P_s(z,t,\lambda_i) = \Gamma n_{eff}/(2hv_i dw v_g)\sqrt{\varepsilon_0/\mu_0}\cdot$

$[|F(z,t,\lambda_i)|^2+|R(z,t,\lambda_i)|^2]$ the photon density distribution of the i^{th} wavelength channel, λ_i is the wavelength of the i^{th} ($i=0,\mp1,\mp2,\ldots,\mp M$) channel in the sliced spectrum, Γ the optical confinement factor, $n_{eff}=n^0_{eff}-\lambda_0/(4\pi)\alpha_{LEF}\Gamma\cdot g(z,t,\lambda_i)$ effective index, n^0_{eff} effective index without injection, λ_0 the peak gain wavelength, α_{LEF} linewidth enhancement factor, $g(z,t,\lambda_i)=a\ln[N(z,t)/N_0][1-0.5(\lambda_i-\lambda_0/\Delta\lambda_G)^2]$ the material optical gain, a the material gain coefficient, N_0 the transparent carrier density, $\Delta\lambda_G$ the gain profile width, h Planck's constant, v_i the optical frequency corresponding to λ_i, d thickness of active region, w width of active region, ε_0 the permittivity of a vacuum, μ_0 the permeability of a vacuum, $F(z,t,\lambda_i)$ the slowly varying envelopes of the forward propagating fields, $R(z,t,\lambda_i)$ the slowly varying envelopes of the backward propagating fields, ε nonlinear gain suppression coefficient, $P_{tot}(z,t)=\sum_{i=-M}^{M}P_s(z,t,\lambda_i)$ the total photon density distribution in all wavelength channel, j the imaginary unit, and α the optical modal loss.

The magnitude of the spontaneous emission noise fields $\tilde{s}^f(z,t,\lambda_i)$ and $\tilde{s}^r(z,t,\lambda_i)$ are approximated as Gaussian random processes with a zero mean and satisfy following autocorrelation function [29]:

$$\left|\tilde{s}^{f,r}(z,t,\lambda_i)\right|\left|\tilde{S}^{f,r}(z',t',\lambda_i')\right| = \gamma\frac{R_{sp}(z,t,\lambda_i)}{d_z v_g}\delta(z-z')\,\delta(t-t')\,\delta(\lambda_i-\lambda_i'), \quad (18)$$

where γ is the spontaneous coupling factor, $R_{sp}(z,t,\lambda_i)$ the spontaneous emission rate, d_z the length of a subsection introduced by the spatial discretization of the active region along the wave propagation direction, and $\delta()$ Dirac's delta function. The phase of the spontaneous emission noise fields is assumed to be uniformly distributed between 0-2π.

Appendix B

The slow-varying envelope of a propagating optical pulse in the fiber can be described by the nonlinear Schrodinger equation (NSE) [32]:

$$\frac{\partial A(z,t)}{\partial z}+\frac{\alpha}{2}A(z,t)+\beta_1\frac{\partial A(z,t)}{\partial t}+\frac{j}{2}\beta_2\frac{\partial^2 A(z,t)}{\partial t^2}-\frac{1}{6}\beta_3\frac{\partial^3 A(z,t)}{\partial t^3}=j\gamma|A(z,t)|^2A(z,t), \quad (19)$$

where A is the low-varying envelope of the optical field, α the fiber loss, β_1 the wave propagation constant, β_2 the second-order dispersion, β_3 the third-order dispersion, γ the fiber nonlinear parameter, and j the imaginary unit.

Transforming to a reference frame moving with the pulse and introducing the new coordinates ($T=t-\beta_1 z$), the term β_1 can be eliminated in (19) to yield:

$$\frac{\partial A(z,T)}{\partial z}+\frac{\alpha}{2}A(z,T)+\frac{j}{2}\beta_2\frac{A(z,T)}{\partial T^2}-\frac{\beta_3}{6}\frac{A(z,T)}{\partial T^3}=j\gamma\left|A^2(z,T)\right|A(z,T). \quad (20)$$

According to the split-step method [34], the solution to (20) is given by:

$$A(z+\Delta z,\omega)=\exp[j(1/2\beta_2\Delta z\omega^2-1/6\beta_3\Delta z\omega^3-1/2\alpha\Delta z)]F[A(z,T)], \quad (21)$$

$$A(z+\Delta z,T)=\exp\left\{j\Delta z\gamma\left|F^{-1}[A(z+\Delta z,\omega)]\right|\right\}\cdot\Delta F^{-1}[A(z+\Delta z,\omega)], \quad (22)$$

where $F[\,]$ and $F^{-1}[\,]$ are the Fourier and inverse Fourier transforms, respectively. In our simulations, we have neglected dispersions higher than the second order as well as the fiber nonlinearity by setting $\gamma=0$, due to the relative short transmission distance. As such, we can rewrite (21) and (22) as:

$$A(z+\Delta z,T)=F^{-1}\left\{\exp\left[\frac{1}{2}\left(j\beta_2\Delta z\omega^2-\alpha\Delta z\right)\right]F[A(z,T)]\right\}. \quad (23)$$

Appendix C

The DFB laser is simulated by a travelling wave model (TWM) [31]:

$$\frac{dN(z,t)}{dt}=\frac{I(t)}{eV}-\frac{N(z,t)}{\tau_c}-\frac{v_g P_s(z,t)\,g(z,t)}{1+\varepsilon P_s(z,t)}, \quad (24)$$

$$\left(\frac{1}{v_g}\frac{\partial}{\partial t}+\frac{\partial}{\partial z}\right)F(z,t)=\left\{-j\delta+\frac{1}{2}\left[\frac{\Gamma g(z,t)}{1+\varepsilon P_s(z,t)}-\alpha\right]\right\}\cdot F(z,t)+j\kappa R(z,t)+\tilde{s}^f(z,t), \quad (25)$$

$$\left(\frac{1}{v_g}\frac{\partial}{\partial t}-\frac{\partial}{\partial z}\right)R(z,t)=\left\{-j\delta+\frac{1}{2}\left[\frac{\Gamma g(z,t)}{1+\varepsilon P_s(z,t)}-\alpha\right]\right\}\cdot R(z,t)+j\kappa F(z,t)+\tilde{s}^r(z,t), \quad (26)$$

where $N(z,t)$ is the carrier density, $I(t)$ the injected current, e the electron charge, V the active region volume, τ_c the carrier lifetime, $v_g=c/n_g$ the group velocity, c the speed of light, n_g the group index, $P_s(z,t)=n_{eff}/(2hv_0)\sqrt{\varepsilon_0/\mu_0}\Gamma/(dwv_g)\cdot[|F(z,t)|^2+|R(z,t)|^2]$ the photon density distribution, $n_{eff}=n^0_{eff}-\lambda_0/(4\pi)\alpha_{LEF}\Gamma g(z,t)$ effective index, n^0_{eff} effective index without injection, λ_0 the peak gain wavelength, α_{LEF} linewidth enhancement factor, Γ the optical confinement factor, $g(z,t)=a\ln[N(z,t)/N_0]$ the material optical gain, a the material gain coefficient, N_0 the transparent carrier density, h Planck's constant, v_0 the optical frequency corresponding to λ_0, ε_0 the permittivity of a vacuum, μ_0 the permeability of a vacuum, d thickness of active region, w width of active region, $F(z,t)$ the slowly varying envelopes of the forward propagating fields, $R(z,t)$ the slowly varying envelopes of the backward propagating fields, ε nonlinear gain suppression coefficient, j the imaginary unit, $\delta=[2\pi n^0_{eff}/\lambda_0-1/2\alpha_{LEF}\Gamma g(z,t)-\pi/\Lambda]$ the phase detuning factor from the Bragg wavelength, Λ Bragg

grating period, α the optical modal loss, and κ grating coupling coefficient.

The magnitude of the spontaneous emission noise fields $\tilde{s}^f(z,t)$ and $\tilde{s}^r(z,t)$ are treated in a similar way as (18) in Appendix A:

$$\left|\tilde{s}^{f,r}(z,t)\right|\left|\tilde{S}^{f,r}(z',t')\right| = 2\sqrt{\frac{\mu_0}{\varepsilon_0}}\frac{\Gamma\Upsilon g_{sp} h v_0}{n_{eff}}\delta(z-z')\,\delta(t-t'), \quad (27)$$

where γ indicates the spontaneous coupling factor, g_{sp} the spontaneous emission gain, and $\delta()$ Dirac's delta function. Again, the phase of the spontaneous emission noise fields is assumed to be uniformly distributed between 0-2π.

The finite bandwidth of the gain profile is modeled by an infinite impulse response (IIR) filter approach [39], [40]:

$$|H(\omega)|^2 = \left\{(1-\eta)^2/\left[1+\eta^2-2\eta cos(\omega\Delta t)\right]\right\}, \quad (28)$$

where η indicates the filter coefficient that controls the filter bandwidth and Δt the time marching step in simulation.

REFERENCES

[1] P. J. Winzer, "Scaling optical fiber networks: Challenges and solutions," *Opt. Photon. News*, vol. 26, no. 3, pp. 28–35, 2015.

[2] M. Chagnon, "Optical communications for short reach," *J. Lightw. Technol.*, vol. 37, no. 8, pp. 1779–1797, Apr. 2019.

[3] G. P. Agrawal, *Fiber Optic Communications Systems*, 4th ed., Hoboken, NJ, USA: Wiley, 2010.

[4] S. Pato, S. Pato, P. Monteiro, P. Monteiro, and H. Silva, "Impact of mode partition noise in the performance of 10 Gbit/s ethernet passive optical networks," in *Proc. 9th Int. Conf. Transp. Opt. Netw.*, Rome, Italy, pp. 67–70, 2007.

[5] K. Ogawa and R. Vodhanel, "Measurements of mode partition noise of laser diodes," *IEEE J. Quantum Electron.*, vol. 18, no. 7, pp. 1090–1093, Jul. 1982.

[6] J. C. Campbell, "Calculation of the dispersion penalty for the route design of single-mode systems," *J. Lightw. Technol.*, vol. 6, no. 10, pp. 564–573, Apr. 1988.

[7] G. P. Agrawal, P. J. Anthony, and T. M. Shen, "Dispersion penalty for 1.3 μm lightwave systems with multimode semiconductor lasers," *J. Lightw. Technol.*, vol. 6, no. 5, pp. 620–625, May 1988.

[8] R. H. Wentworth, G. E. Bodeep, and T. E. Darcie, "Laser mode partition noise in lightwave systems using dispersive optical fiber," *J. Lightw. Technol.*, vol. 10, no. 1, pp. 84–89, Jan. 1992.

[9] T. P. Lee, C. A. Burrus, G. Eisenstein, and W. B. Sessa, "Amplifier-modulator integrated with a cleaved-coupled-cavity injection laser," *Electron. Lett.*, vol. 20, no. 15, pp. 625–627, Jul. 1984.

[10] W. T. Tsang, N. A. Olsson, and R. A. Logan, "Stable ssingle-longitudinal-mode operation under high-speed direct modulation in cleaved-coupled-cavity GaInAsP semiconductor lasers," *Electron. Lett.*, vol. 19, no. 13, pp. 488–490, Jun. 1983.

[11] B. Corbett and D. McDonald, "Single longitudinal mode ridge waveguide 1.3μm Fabry-Perot laser by modal perturbation," *Electron. Lett.*, vol. 31, no. 25, pp. 2181–2182, 1995.

[12] Y. Wang, Y. Yang, S. Zhang, L. Wang, and J. -J. He, "Narrow linewidth single-mode slotted Fabry–Pérot laser using deep etched trenches," *IEEE Photon. Technol. Lett.*, vol. 24, no. 14, pp. 1233–1235, Jul. 2012.

[13] X. Li, Z. -S. Zhu, Y. -P. Xi, L. Han, C. Ke, and Y. Pan, "Single-mode Fabry-Perot laser with deeply-etched slanted double trenches," *Appl. Phys. Lett.*, vol. 107, no. 9, Sep. 2015 , Art. no. 091108.

[14] D. Hjelme and A. Mickelson, "On the theory of external cavity operated single-mode semiconductor lasers," *IEEE J. Quantum Electron.*, vol. QE-23, no. 6, pp. 1000–1004, 1987.

[15] H. C. Kwon and S. K. Han, "Performance analysis of a wavelength-locked Fabry-Perot laser diode by light injection of an external spectrally sliced Fabry-Perot laser diode," *Appl. Opt.*, vol. 45, pp. 6175–6179, 2006.

[16] K. Sato and H. Toba, "Reduction of mode partition noise by using semiconductor optical amplifiers," *IEEE J. Sel. Topics Quantum Electron.*, vol. 7, no. 2, pp. 328–333, Mar./Apr. 2001.

[17] M. Mielke, P. J. Delfyett, and G. A. Alphonse, "Suppression of mode partition noise in a multiwavelength semiconductor laser through hybrid mode locking," *Opt. Lett.*, vol. 27, pp. 1064–1066, 2002.

[18] J. W. Fu, "Narrow spectral width FP lasers for high-speed short-reach applications," *J. Lightw. Technol.*, vol. 34, no. 21, pp. 4898–4906, 2016.

[19] K. Kikuchi, "Fundamentals of coherent optical fiber communications," *J. Lightw. Technol.*, vol. 34, no. 1, pp. 157–179, 2016.

[20] G. P. Agrawal, *Semiconductor Lasers*, 2th ed. New York, NY, USA: Springer, 1993.

[21] K. Petermann, *Laser Diode Modulation and Noise*, 1st ed. New York, NY, USA: Springer, 1991.

[22] D. Marcuse, "Computer simulation of laser photon fluctuations: Single-cavity laser results," *J. Quantum Electron*, vol. 20, no. 10, pp. 1148–1155, Oct. 1984.

[23] W. H. Press *et al.*, *Numerical Recipes in C*, 2nd ed. Cambridge, U.K.: Cambridge Univ. Press, 1992.

[24] M. Ettenberg, "Control of facet damage in GaAs laser diodes," *Appl. Phys. Lett.*, vol. 18, no. 12, pp. 571–573, 1971.

[25] N. H. Jensen, "Partition noise in semiconductor lasers under cw and pulsed operation," *IEEE J. Quantum Electron.*, vol. QE-23, no. 1, pp. 71–79, Jan. 1987.

[26] K. Ogawa and R. Vodhanel, "Measurements of mode partition noise of laser diodes," *IEEE J. Quantum Electron.*, vol. 18, no. 7, pp. 1090–1093, Jul. 1982.

[27] *10-Gigabit-capable passive optical networks (XG-PON): Physical media dependent (PMD) layer specification*, ITU-T Standard G.987.2, 2016.

[28] J. Park, X. Li, and W. P. Huang, "Performance simulation and design optimization of gain-clamped semiconductor optical amplifiers based on distributed Bragg reflectors," *IEEE J. Quantum Electron.*, vol. 39, no. 11, pp. 1415–1423, Nov. 2003.

[29] J. Park, X. Li, and W. P. Huang, "Comparative study of mixed frequency-time-domain models of semiconductor laser optical amplifiers," *IEE Proc.-Optoelectron*, vol. 152, no. 3, pp. 151–159, Jun. 2005.

[30] M. J. Connelly, "Wideband semiconductor optical amplifier steady-state numerical model," *IEEE J. Quantum Electron.*, vol. 37, no. 3, pp. 439–447, Mar. 2001.

[31] X. Li, *Optoelectronic Devices: Design, Modeling, and Simulation*. Cambridge, U.K.: Cambridge Univ. Press, 2009.

[32] G. P. Agrawal, *Nonlinear Fiber Optics*, 3rd ed. New York, NY, USA: Academic, 2001.

[33] O. V. Sinkin, R. Holzlohner, J. Zweck, and C. R. Menyuk, "Optimization of the split-step Fourier method in modeling optical fiber communication systems," *J. Lightw. Technol.*, vol. 21, no. 1, pp. 61–68, Jan. 2003.

[34] R. H. Hardin and F. D. Tappert, "Applications of the split step Fourier method to the numerical solution of nonlinear and variable coefficient wave equations," *SIAM Rev. Chronicle*, vol. 15, 1973, Art. no. 423.

[35] J. Hancock, "Jitter—Understanding it, measuring it, eliminating it, part 1: Jitter fundamentals," *High Freq. Electron.*, pp. 44–50, 2004.

[36] *Physical Layer and Management Parameters for Serial 25 Gb/s Ethernet Operation Over Single-Mode Fiber*, IEEE Standard 802.3cc, 2017.

[37] D. -Y. Wu, F. -B. Meng, R. Li, R. -S. Liu, and F. Wu, "Passive optical network system performance analysis using a 10 Gbit/s DML," *Appl. Mech. Mater.*, vol. 635-637, pp. 1094–1097, 2014.

[38] R. A. Salvatore, R. T. Sahara, M. A. Bock, and I. Libenzon, "Electroabsorption modulated laser for long transmission spans," *IEEE J. Quantum Electron.*, vol. 38, no. 5, pp. 464–476, May 2002.

[39] D. J. Jones, L. M. Zhang, J. E. Carroll, and D. D. Marcenac, "Dynamics of monolithic passively mode-locked semiconductor lasers," *IEEE J. Quantum Electron.*, vol. 31, no. 6, pp. 1051–1058, Jun. 1995.

[40] J. Zhao, K. Shi, Y. Yu, and L. P. Barry, "Theoretical analysis of tunable three-section slotted Fabry-Perot lasers based on time-domain traveling-wave model," *IEEE J. Sel. Topics Quantum Electron.*, vol. 19, no. 5, pp. 1–8, Sep./Oct. 2013.